INTERNATIONAL JOURNAL FOR NUMERICAL METHODS IN FLUIDS
Int. J. Numer. Meth. Fluids **29**: 849–864 (1999)

NUMERICAL SOLUTION FOR LAMINAR MIXED CONVECTION IN A HORIZONTAL ANNULAR DUCT: TEMPERATURE-DEPENDENT VISCOSITY EFFECT

C. NOUAR*

LEMTA, UMR 7563 (CNRS-UHP-INPL), 2 Avenue de la Forêt de Haye, BP 160, 54504 Vandoeuvre-lès-Nancy Cedex, France

SUMMARY

The influence of free convection and variable viscosity on forced laminar flow of a Newtonian fluid in a horizontal annular duct is investigated. The inner and outer cylinders are subjected to a constant heat flux density. At the entrance of the annular duct, the flow is fully developed and the temperature profile is uniform. The Prandtl and Boussinesq hypothesis were adopted. The continuity equation and the three-dimensional parabolized form of the momentum and energy equations are solved numerically using finite differences. Near the entrance section, forced convection is the dominant mechanism. Further downstream, the fluid heats up and buoyancy becomes more important. The fluid near the walls is warmer, and therefore lighter than the fluid in the central part of the annular space; it therefore flows upward along the walls. A continuity requires a downflow of the heavier fluid between the two cylinders. This secondary flow modifies the structure of the dynamic and thermal fields. The numerical results show that a decrease in fluid viscosity with temperature leads to: (i) an increase in axial velocity in the upper part of the annular duct and a decrease in the lower part; (ii) a rise in the secondary flow intensity; (iii) a reduction in temperature difference between the upper and lower parts of a cylinder; (iv) an increase of the overall heat transfer coefficient. Copyright © 1999 John Wiley & Sons, Ltd.

KEY WORDS: mixed convection; annular duct; variable viscosity; numerical calculation

1. INTRODUCTION

Laminar mixed convection in a horizontal circular duct has been studied by several workers since the paper published in 1959 by Morton [1], where an analytical solution based on a perturbation method was proposed. The case of an annular geometry has been however, much less studied, even though this geometry is the most often encountered in fluid thermal processes. Most articles dealing with mixed convection in horizontal annular ducts only consider the case where the dynamic and the thermal patterns are fully developed with different types of boundary conditions. Mojtabi and Caltagirone [2] considered the case of inner and outer cylinders at constant temperatures, Nieckele and Patankar [3], Kotake and Hattori [4], as well as Ciampi *et al.* [5] examined the case where the inner cylinder is heated at constant flux and the outer cylinder is adiabatic. Recently, Thermina *et al.* [6] studied the simultaneously developing mixed convection flow and heat transfer for fluids with Prandtl

* Correspondence to: LEMTA, UMR 7563 (CNRS-UHP-INPL), 2 Avenue de la Forêt de Haye, BP 160, 54504 Vandoeuvre-lès-Nancy Cedex, France. E-mail: cnouar@ensem.u-nancy.fr

CCC 0271–2091/99/070849–16$17.50

Received December 1997
Revised March 1998

number close to unity. The elliptic formulation is retained: the axial viscous and thermal diffusions are not neglected. The inner cylinder is heated at constant temperature and the outer one is maintained at the entrance temperature. These authors mentioned the possibility of axial reverse flow when natural convection is sufficiently intense. The literature shows also that few works take the variation of viscosity with temperature into consideration, whereas the majority of fluids used in industrial processes have such property. Hong and Bergles [7] investigated theoretically the heat transfer for fluids with high Prandtl number flowing in a circular duct heated with a constant heat flux. The dynamic and thermal fields are considered fully developed. It is assumed that the flow in a straight section of the duct consists of two regions: a region close to the wall that corresponds to a developing boundary layer originating from the lower part of the duct and growing along the circumference, and a central region where the axial flow is undisturbed. The authors showed that the reduction of the viscosity with temperature reduces the thickness of the circumferential boundary layer and creates a stronger secondary flow. Chou and Tung [8] performed a numerical study of the heat transfer for mineral oil in a rectangular duct. The different mechanisms governing the heat transfer in the entrance region are clearly explained. However, the effect of viscosity thermodependency on the mixed convection is not set obviously. In other investigations (Bishop and Deshpande [9], Shome and Jensen [10]), the effect of variable viscosity on free convection is just incorporated into the viscosity ratio correction term for Nusselt or friction factor correlation.

To the knowledge of the auhtor, there is no study that clearly brings out the effect of the thermodependence of the viscosity on the dynamic and thermal fields structure for a mixed convection in a horizontal axisymmetric geometry. In the present investigation, a laminar mixed convection in a horizontal annular duct is studied. The inner and outer cylinders' walls are heated at a constant heat flux density ϕ.

As the fluid enters the annular duct, a thermal boundary layer develops on the walls of the cylinders, with a secondary flow developing inside the thermal boundary layer due to the temperature difference between the walls and the inlet fluid. Since the viscosity of the fluid decreases with temperature, the fluid is then accelerated near the heated wall and decelerated in the central part of the annular duct for flow conservation. This motion generates node-like sinks along the walls of the annular duct and causes fluid particles to move towards the wall. Simultaneously, the displacement of the secondary boundary layer induces a downward stream between the two cylinders. As explained by Yao [11], the axial velocity profile turns to accommodate the downward stream generated by the displacement of the secondary boundary layer. The component of the axial pressure gradient induced by the secondary flow is negative along the bottom of the duct and is positive along the top. The upward flow of the warmer fluid near the heated walls, and the downward flow of the cooler fluid between the cylinders leads to a stratification of a fluid in a section of the annular duct. The heat transfer is then enhanced in the bottom and downgraded on the top. The decrease of the viscosity with temperature on one hand leads to the reduction of the drag forces of viscous origin, therefore, to the intensification of the secondary flow, and on the other hand, increases the wall axial velocity gradient, which diminishes the wall temperature and consequently the buoyancy force. It will be shown that: (i) contrary to the case of constant viscosity, the fluid will be accelerated in the upper part and decelerated in the lower part when it is sufficiently thermodependent. The axial flow in the central region is strongly disturbed even for a large Prandtl number, contrary to the assumptions of Hong and Bergles [7]; (ii) the temperature difference between the top and the bottom of a cylinder is reduced; and (iii) the secondary flow intensity increases.

The plan of this paper is as follows. The formulation of the problem through the governing equations is given in Section 2. The procedure for obtaining a numerical solution is described

in Section 3. The numerical results are analyzed in Section 4. Finally, some conclusions are drawn about the effect of thermodependency of viscosity on the dynamic field structure for a mixed convection in a horizontal axisymmetric geometry.

2. PROBLEM FORMULATION

A laminar flow of a Newtonian fluid in a horizontal annular duct is considered. The inner and outer cylinders, of radius R_1 and R_2 respectively, are subjected to a constant heat flux density ϕ (Figure 1). The ratio R_1/R_2 will be designated as R. The variations of the fluid density and viscosity with temperature are assumed to be given by:

$$\rho = \rho_e[1 - \beta(T - T_e)], \qquad \mu = a \exp(-bT), \tag{1}$$

where, ρ_e is the fluid density at the entrance temperature T_e and β is the thermal expansion coefficient. The specific heat C_p and the thermal conductivity λ are assumed constant. The formulation presented below is written for an incompressible fluid under the following assumptions: (i) the flow is steady; (ii) the Peclet number is sufficiently large ($Pe > 100$) so as the diffusion in the axial direction (main flow) can be neglected in the momentum and energy equations; (iii) the variation of the density with temperature is taken into consideration only in the buoyancy term (Boussinesq approximation); (iv) the viscous dissipation is negligible. The dimensionless equations governing the conservation of mass, momentum and energy are:

$$\vec{V} \cdot \vec{\nabla} = 0, \tag{2}$$

$$[\vec{V} \cdot \vec{\nabla}]u = -\frac{dP_m}{dz} + \frac{1}{Re}\bar{\mu}\Delta u + \frac{1}{Re}\left[\frac{\partial \bar{\mu}}{\partial r}\frac{\partial u}{\partial r} + \frac{1}{r^2}\frac{\partial \bar{\mu}}{\partial \theta}\frac{\partial u}{\partial \theta}\right], \tag{3}$$

$$\begin{aligned}[\vec{V} \cdot \vec{\nabla}]w + \frac{vw}{r} = &-\frac{1}{r}\frac{\partial P'}{\partial \theta} + \frac{1}{Re}\bar{\mu}\left[\Delta w + \frac{2}{r^2}\frac{\partial v}{\partial \theta} - \frac{w}{r^2}\right] + \frac{Gr}{Re^2}\Theta \sin\theta \\ &+ \frac{1}{Re}\left[\left(\frac{\partial w}{\partial r} - \frac{w}{r} + \frac{1}{r}\frac{\partial v}{\partial \theta}\right)\frac{\partial \bar{\mu}}{\partial r} + \frac{2}{r}\left(\frac{v}{r} + \frac{1}{r}\frac{\partial w}{\partial \theta}\right)\frac{\partial \bar{\mu}}{\partial \theta} + \frac{1}{r}\frac{\partial \bar{\mu}}{\partial z}\frac{\partial u}{\partial \theta}\right],\end{aligned} \tag{4}$$

$$[\vec{V} \cdot \vec{\nabla}]v - \frac{w^2}{r} = -\frac{\partial P'}{\partial r} + \frac{1}{Re}\bar{\mu}\left[\Delta v - \frac{2}{r^2}\frac{\partial w}{\partial \theta} - \frac{v}{r^2}\right] - \frac{Gr}{Re^2}\Theta \cos\theta$$

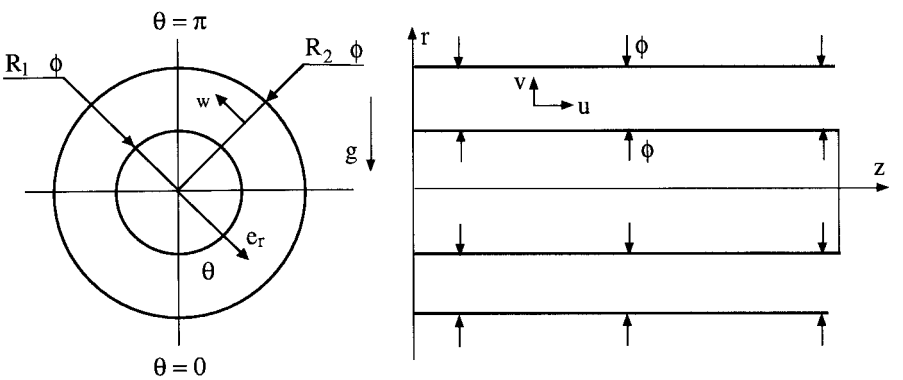

Figure 1. Flow geometry and co-ordinate system.

$$+\frac{1}{Re}\left[2\frac{\partial v}{\partial r}\frac{\partial \bar{\mu}}{\partial r}+\frac{1}{r}\left(\frac{\partial w}{\partial \theta}-\frac{w}{r}+\frac{1}{r}\frac{\partial v}{\partial \theta}\right)\frac{\partial \bar{\mu}}{\partial \theta}+\frac{\partial \bar{\mu}}{\partial z}\frac{\partial u}{\partial r}\right], \tag{5}$$

$$[\vec{V}\cdot\vec{\nabla}]\Theta=\frac{1}{Pe}\Delta\Theta. \tag{6}$$

To ensure that the volume of fluid flowing across each cross-stream plane is conserved, the governing equations, (2)–(6), are to be solved along with the integral continuity equation given by:

$$\int_0^{\pi}\int_R^1 ru\ \mathrm{d}r\ \mathrm{d}\theta=\frac{\pi}{2}[1-r^2], \tag{7}$$

where u, v and w are the axial, radial and azimuthal components respectively of $\vec{V}$.

$$\vec{V}=[u, v, w]^t; \qquad \Delta=\left[\frac{\partial^2}{\partial r^2}+\frac{1}{r}\frac{\partial}{\partial r}+\frac{1}{r^2}\frac{\partial^2}{\partial \theta^2}\right] \quad \text{and} \quad [\vec{V}\cdot\vec{\nabla}]=\left[u\frac{\partial}{\partial z}+v\frac{\partial}{\partial r}+\frac{w}{r}\frac{\partial}{\partial \theta}\right].$$

At the entrance section, the flow is fully developed and the temperature profile uniform. Furthermore, the flow is assumed to be symmetrical with respect to the vertical plane containing the duct axis. The boundary conditions are given by:

$$r=R: \quad u=v=w=0, \qquad \frac{\partial\Theta}{\partial r}=-1/(1-R); \tag{8}$$

$$r=1: \quad u=v=w=0, \qquad \frac{\partial\Theta}{\partial r}=-1/(1-R); \tag{9}$$

$$z=0: \quad u=u_{\mathrm{fd}}, \qquad v=w=\Theta=0; \tag{10}$$

$$\theta=0,\ \pi; \qquad \frac{\partial u}{\partial \theta}=\frac{\partial v}{\partial \theta}=\frac{\partial\Theta}{\partial \theta}=w=0. \tag{11}$$

In Equations (2)–(11), the variables have been rendered dimensionless using a length R_2, a velocity U_{d} (mean axial velocity), a reference viscosity μ_{e} and a pressure $\rho_{\mathrm{e}}U_{\mathrm{d}}^2$. The dimensionless temperature is defined as: $\Theta=(T-T_{\mathrm{e}})/\Delta T$ with $\Delta T=\phi D_{\mathrm{h}}/2\lambda$, D_{h} is the hydraulic diameter. The Peclet number Pe, Grashof number Gr, and the Reynolds number Re are defined as:

$$Pe=\rho C_p U_{\mathrm{d}} R_2/\lambda; \qquad Re=\rho U_{\mathrm{d}} R_2/\mu_{\mathrm{e}}; \qquad Gr=\rho_{\mathrm{e}}^2 g\beta\Delta T R_2^3/\mu_{\mathrm{e}}^2.$$

The pressure distribution in general, can be obtained by deriving a Poisson pressure equation from the momentum equations. The application of this procedure without modification in this instance will produce a fully elliptic pressure equation, therefore resulting in an inconsistency with earlier treatment of the momentum equations. The fully parabolized governing equations may be obtained (Patankar and Spalding [12]) by setting: $P=P_m(z)+P'(r,\theta,z)$ under the assumption of $\mathrm{d}P_m/\mathrm{d}z \gg \partial P'/\partial r$, $(1/r)\partial P'/\partial\theta$, $\partial P'/\partial z$. The resulting changes in conservation momentum equations are:

$$\partial P/\partial z \to \mathrm{d}P_m/\mathrm{d}z, \qquad \partial P/\partial r \to \partial P'/\partial r, \qquad \partial P/\partial\theta \to \partial P'/\partial\theta.$$

The pressure P_m can be appropriately viewed as a space-averaged pressure over a cross-section. The principal drawback of this model is that it does not allow for flow recirculation in the axial direction.

Using the dimensionless temperature Θ, $\bar{\mu}$ can be written as: $\bar{\mu}=\exp(-Pn\Theta)$, where Pn is the Pearson number: $Pn=b\phi D_{\mathrm{h}}/2\lambda$. Then, the problem of mixed convection depends on five

dimensionless numbers: R, Re, Pr, Gr and Pn. To formulate the local heat transfer between the cylinder wall and the fluid, internal and external Nusselt numbers Nu_1 and Nu_2 respectively, are introduced:

– Local Nusselt number (depends on z and θ):

$$Nu_{1,2} = 2/[\Theta_{1,2} - \Theta_m].$$

– Averaged circumferentially Nusselt number (depends on z)

$$Nu_{\text{moy}} = 2/[\Theta_{1,2\text{moy}} - \Theta_m], \quad \text{where} \quad \Theta_{1,2\text{moy}} = (1/\pi)\int_0^{\pi} \Theta_{1,2}\, \mathrm{d}\theta.$$

Θ_m is the dimensionless bulk temperature and $\Theta_{1,2\text{moy}}$ is the circumferentially averaged wall temperature (inner or outer cylinder). The trapezoidal's rule is used to compute the average $\Theta_{1,2\text{moy}}$.

3. NUMERICAL SOLUTION

Equations (3)–(6) constitute a parabolic system and can be solved by a stepwise integration in the axial direction from specified set of upstream initial conditions. The conservation equations with the associated boundary conditions are discretized using finite differences. The partial derivatives in the radial and azimuthal directions are approximated by a centered scheme, the first-order derivatives in the axial direction are approximated by an upwind scheme. The finite difference equations are linearized by assuming that when the product of two unknowns occurs, one of them is given approximately by its value at the previous axial step. The procedure for the solution to the momentum and energy equations is based on the one proposed by Briley [13]. It starts by solving the finite difference form of the z momentum equation for the u field assuming $\mathrm{d}P_m/\mathrm{d}z$. Based on this u field, the overall continuity requirement of specified mass flow rate is checked. The residual mass defined in Equation (12) coupled with a secant method is used iteratively in correcting the u field and P_m. The secant method converges in the limit of machine accuracy in three iterations.

$$\int_0^{\pi}\int_R^1 ru\, \mathrm{d}r\, \mathrm{d}\theta = \frac{\pi}{2}[1 - R^2] = \text{Res}. \tag{12}$$

When the residual flow rate Res, calculated using the Simpson rule, is less than or equal to 10^{-7}, the constraint (12) is assumed verified. The next step is the computation of the cross-stream velocities v and w from the momentum equations in the r- and θ-directions using a pressure field $P'(r, \theta, z)$ of the upstream section. The results v_{p} and w_{p} (provisional velocity) are then considered to check the local continuity requirement. To this end, the following decomposition of v and w is performed:

$$v = v_{\text{p}} + v^*; \qquad w = w_{\text{p}} + w^*, \tag{13}$$

where v^* and w^* are corrections to v_{p} and w_{p} which ensure that v and w satisfy the continuity equation. It is assumed that the correction velocities are irrotational. Therefore, there exists a potential φ such that:

$$v^* = \frac{\partial \varphi}{\partial r}; \qquad w^* = \frac{1}{r}\frac{\partial \varphi}{\partial \theta}. \tag{14}$$

If Equations (13) and (14) are substituted in Equation (2), a Poisson equation is generated:

$$\Delta\varphi = f, \tag{15}$$

with homogeneous Neumann boundary conditions ($\partial\varphi/\partial n = 0$) on the boundary of the domain $[R, 1] \times [0, \pi]$. The pressure field $P'(r, \theta, z)$ is obtained by constructing a Poisson equation from Equations (4) and (5):

$$\Delta P' = F. \tag{16}$$

The boundary conditions are all of Neumann type. They are derived from r and θ momentum equations. The pressure equation with the boundary conditions is solved on a computational domain formed by grid points one mesh length away from the walls. After the flow variables are computed, the energy equation is solved for the temperature field. As the viscosity varies with temperature, the foregoing procedure is repeated until successive temperature fields do not show significant changes.

Having examined the global procedure for the resolution of the problem, in the following some details are given about the discretization of the governing equations. The momentum and energy equations are discretized using the ADI technique. The tridiagonal system of linearized equations arising from each half step are solved using the Thomas algorithm. The Poisson equations for the potential φ and for the pressure with the corresponding boundary conditions are solved by line under successive relaxation with alternating sweeping direction. The criterion of convergence is $\max|\varphi^{n+1} - \varphi^n|/\max|\varphi^{n+1}| \leq 10^{-5}$, n is the iteration number, and $\max|P'^{n+1} - P'^n|/\max|P'^{n+1}| \leq 10^{-3}$. However, in order to satisfy the divergence theorem, the source terms f and F are replaced respectively, at every grid point by:

$$f_c = f + \frac{1}{S}\left[\int_S f \,\mathrm{d}s - \oint_C (\partial\phi/\partial n)\,\mathrm{d}c\right] \quad \text{and} \quad F_c = F + \frac{1}{S}\left[\int_S F \,\mathrm{d}s - \oint_C (\partial P'/\partial n)\,\mathrm{d}c\right],$$

where, C is the closed boundary of the solution domain of area S and n is the outward normal to C. In the current calculations, the Poisson equations (15) and (16) are written using conservative spatial derivatives. Finally, the overall algorithm is of the order $(\Delta z^2, \Delta r^2, \Delta\theta^2)$.

Calculations were made for a radii ratio, $R = 0.5$. The computations in the present work were performed on a RISC workstation. The CPU time is about 6 h. The results presented in this paper were generated from a regular grid 101×101 in (r, θ)-directions. The axial step was constant and equal to $2.5 \times 10^{-4}/R_2$. In general, the computations were terminated at $z = 150$, where for the working conditions considered here, the dynamic regime is nearly established.

As there is no experimental data or analytical solution corresponding to the mixed convection flow under consideration, the program is validated by comparison with analytical solution for pure forced convection ($Gr = 0$), constant viscosity ($b = 0$), one cylinder heated and the other one adiabatic. In the thermally developing region, the evolution of the circumferentially averaged Nusselt number at the outer cylinder for increasing grid size from 21×21 to 101×101 is plotted in Figure 2. It is compared with the analytical solution of Worsoe-Schmidt [14].

$$Nu = 1.034(1 - R)^{1/3}(\mathrm{d}u/\mathrm{d}r)_{r=1}^{1/3}(X^+)^{-1/3},$$

where, X^+ is the Cameron number: $X^+ = z/Pe$. As can be expected, the successive refinement of the grid takes us asymptotically towards the correct solution. Near the entry section, the thermal boundary layer is very thin. This is why the large grid is not adequate to describe the thermal field near the entry section.

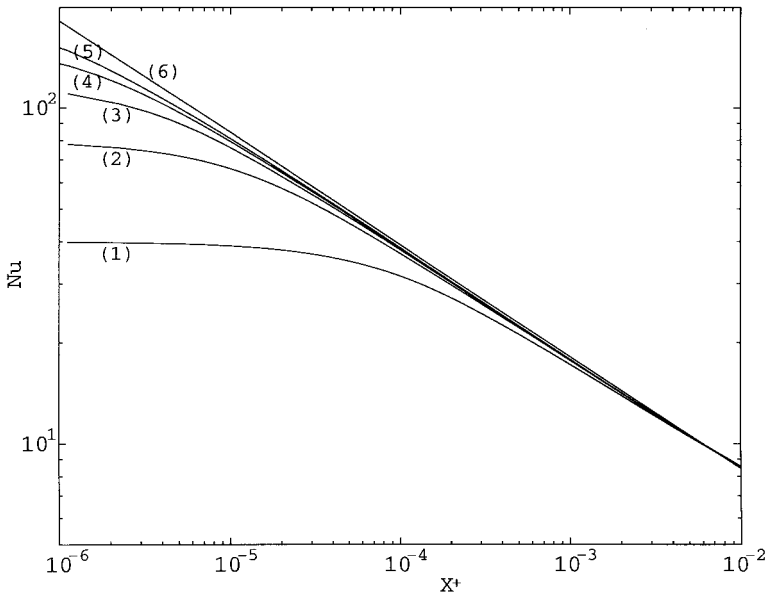

Figure 2. Effect of grid size on the circumferentially averaged Nusselt number: $Re = 32$; $Pr = 348.3$; $Gr = 0$; $Pn = 0$; $\phi_1 = 0$, $\phi_2 = 6000$ W m^{-2}; (1) 21×21, (2) 41×41, (3) 61×61, (4) 81×81, (5) 101×101, (6) analytical solution of Worsoe-Schmidt.

4. ANALYSIS OF RESULTS AND DISCUSSION

The results are basically divided into three parts. In part one, the case of forced convection with variable viscosity is considered. Part two concerns mixed convection with constant viscosity. The case of mixed convection with variable viscosity is presented in part three.

In the case of forced convection coupled with reducing viscosity due to the temperature, there is a reorganization of the flow characterized by an increase in wall velocity gradient on the inner and outer cylinders. This increase is higher at the outer one, where the wall temperature is more important than that on the inner one. The axial velocity in the central zone of the annular gap decreases to maintain the flow conservation. This result is illustrated in Figure 3, where axial velocity profiles are presented at four axial positions. One notes that the rate of deformation of the axial velocity profile is larger in the region near the thermal entrance, such as z from 0 to 12.5, than that near the fully developed region, such as from 37.5 to 125. This flow reorganization is accompanied by the appearance of a radial component of the velocity, directed globally from the central part of the annular gap towards the heated walls. Its intensity decreases along the heating zone since the rate of axial velocity deformation decreases. The flow is axisymmetrical. The isotherms and the axial velocity contours are concentric. As far as the heat transfer is concerned, Figure 4 shows the evolution of the external Nusselt number along the heating zone for $Pn = 0$ and 10. As expected, the heat transfer is enhanced by the decrease of μ with T. A similar evolution is obtained for the internal Nusselt number.

The case of mixed convection when the viscosity remains constant is considered next. As a result of the decrease of the density with temperature, the warmer fluid moves upward ($v > 0$) along the heated walls of the cylinders and the cooler fluid moves downward ($v < 0$) in the core region between the cylinders, as shown in Figure 5. Hence, the flow in a section of the annular

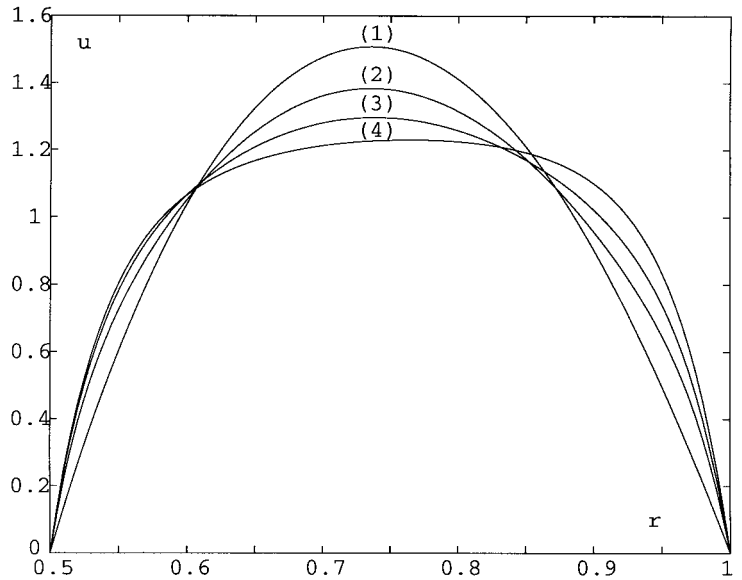

Figure 3. Axial velocity profiles along the heating zone: $Re = 32$; $Pr = 348.3$; $Gr = 0$; $Pn = 10$; (1) $z = 0$, (2) $z = 12.5$, (3) $z = 37.5$, (4) $z = 125$.

gap can be characterized by two counter rotating cells. The analysis of tangential velocity profiles at a given axial position and for different angular positions shows that the fluid is first accelerated between the lower part and the median plane; it is then decelerated between the median plane and the upper part of the duct. Figure 6 shows the evolution of the tangential velocity profile at $\theta = \pi/2$ and for different axial positions. It illustrates the development of the

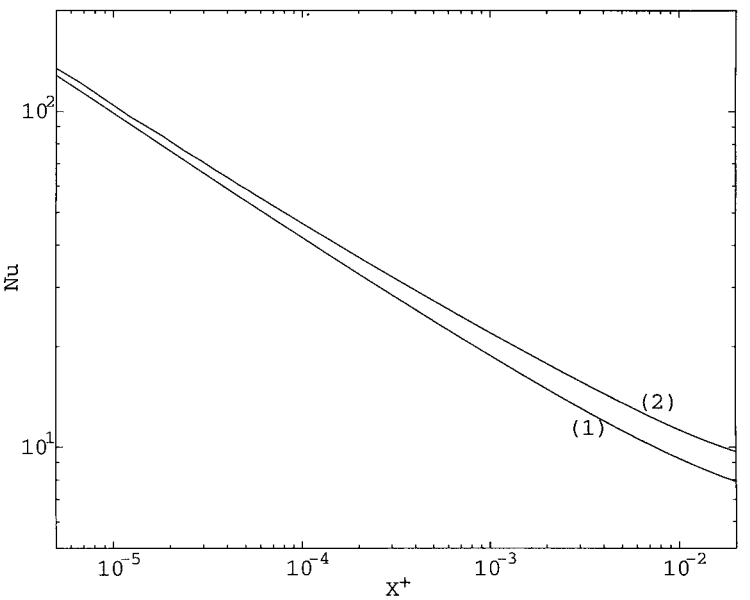

Figure 4. Evolution of the external Nusselt along the heating zone: $Gr = 0$; (1) $Pn = 0$, (2) $Pn = 10$.

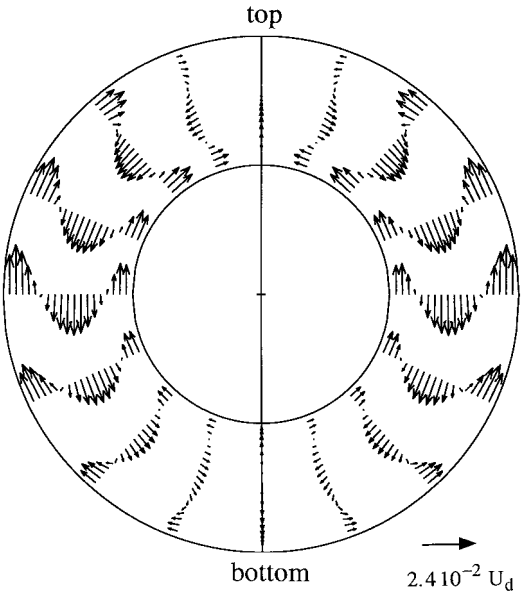

Figure 5. Secondary flow structure: $Re = 35$; $Pr = 557.3$; $Pn = 0$; $\phi_1 = \phi_2 = 6000$ W m^{-2}; $Gr = 6000$; z = 75.

secondary flow along the heating zone. The tangential velocity profile at $z = 125$ is not represented, it is practically identical to that at $z = 75$. The azimuthal flow starts at a short distance from the entrance, then increases and tends toward an asymptotic profile. As suggested by Hong and Bergles [7], the radial position of the maximum of the tangential velocity corresponds to the thickness δ_θ of the circumferentially boundary layer. This defini-

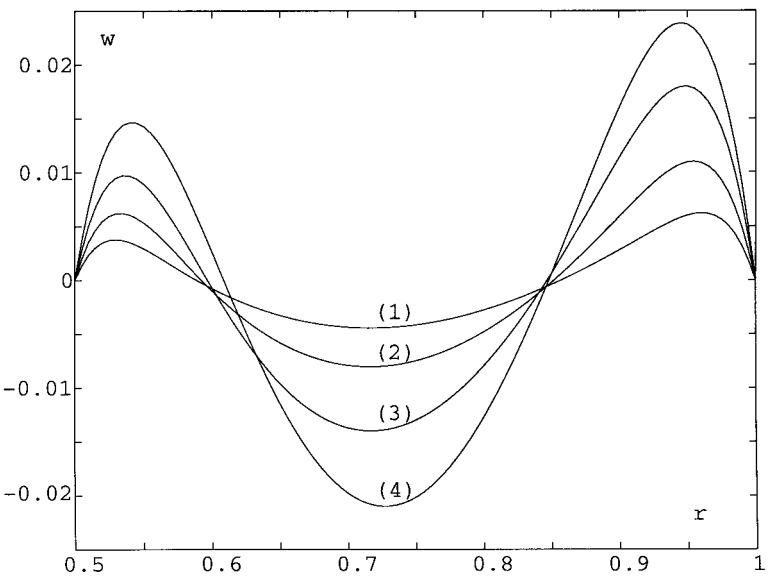

Figure 6. Evolution of the tangential velocity profiles along the heating zone: $Re = 35$; $Pr = 557.3$; $Gr = 6000$; (1) $z = 6.25$, (2) $z = 12.5$, (3) $z = 25$, (4) $z = 75$.

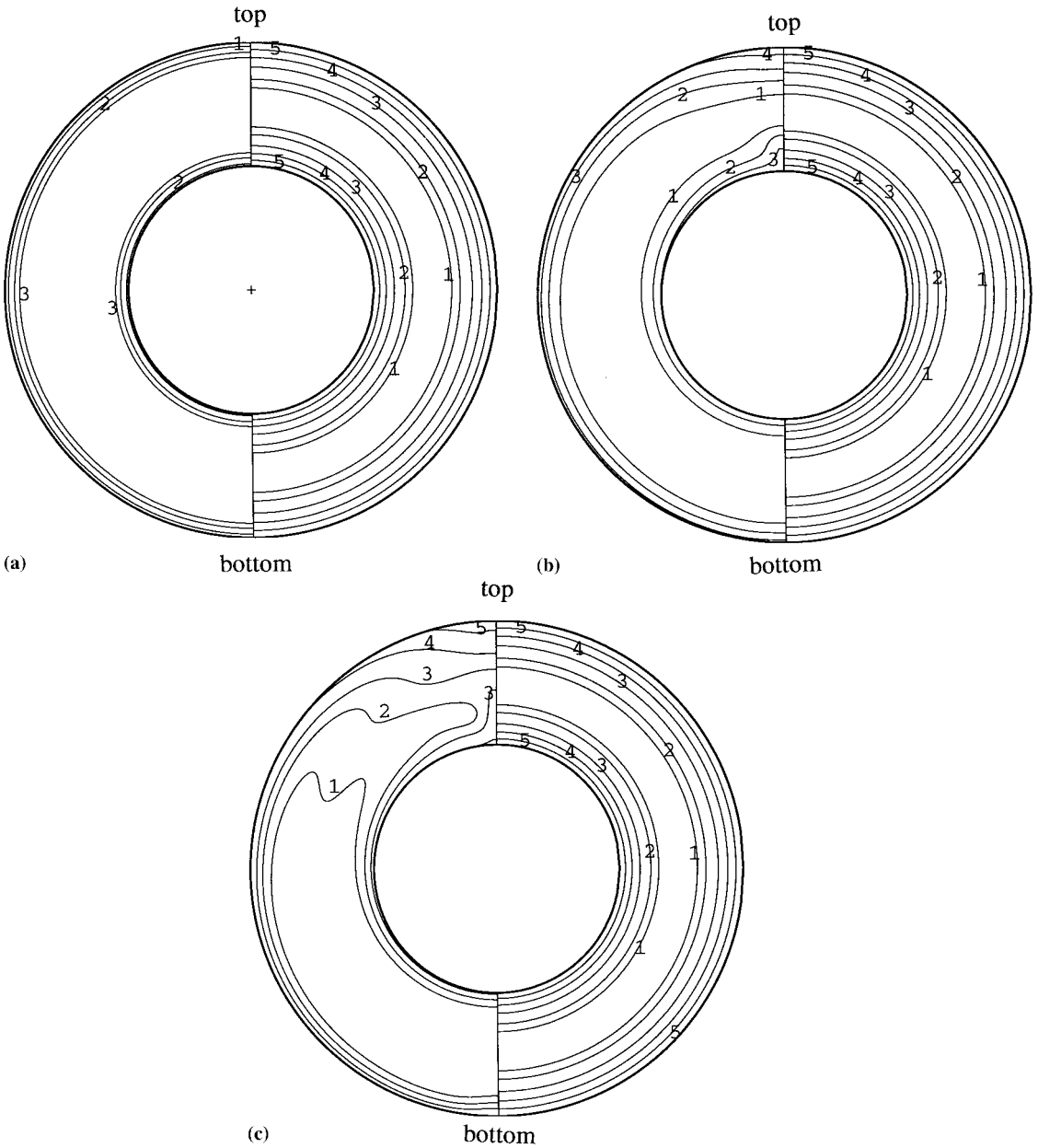

Figure 7. Isotherms (left-hand-side) and axial velocity contours (right-hand-side): $Re = 35$; $Gr = 6000$; $Pr = 557.3$; $Pn = 0$. (a) $z = 6.25$; isotherms (iso Θ^*): $\Theta^* = (\Theta - \Theta_e)/(\Theta_{max} - \Theta_e)$: $\Theta_{max} - \Theta_e = 0.1$: (1) 0.7, (2) 0.3, (3) 0.1; iso-axial velocity (iso u/U_{max}): $U_{max} = 1.5$: (1) 0.9, (2) 0.8, (3) 0.6, (4) 0.4, (5) 0.2. (b) $z = 50$; isotherms: $\Theta_{max} - \Theta_e = 0.28$: (1) 0.1, (2) 0.3, (3) 0.5, (4) 0.8; iso-axial velocity: $U_{max} = 1.5$: (1) 0.9, (2) 0.8, (3) 0.6, (4) 0.4, (5) 0.2. (c) $z = 125$; isotherms: $\Theta_{max} - \Theta_e = 0.41$: (1) 0.1, (2) 0.2, (3) 0.3, (4) 0.5, (5) 0.8; iso-axial velocity: $U_{max} = 1.5$: (1) 0.9, (2) 0.8, (3) 0.6, (4) 0.4, (5) 0.2.

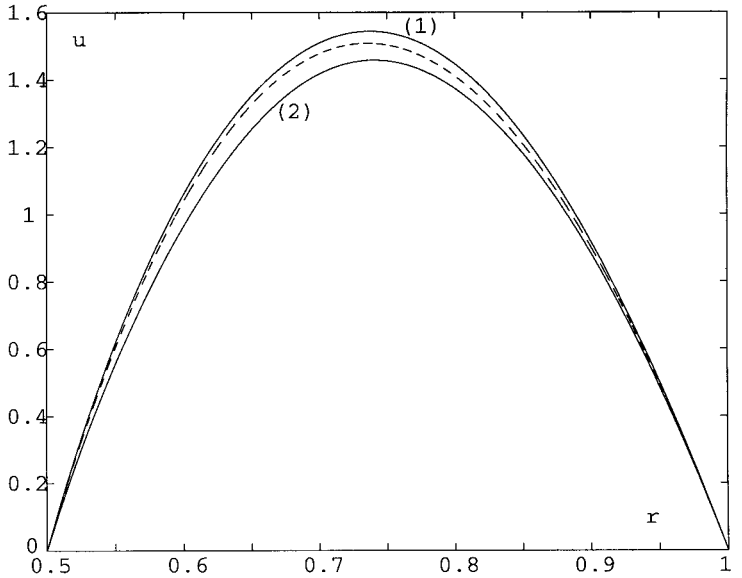

Figure 8. Axial velocity profiles along a central vertical line: case of constant viscosity. $Gr = 9.6 \times 10^4$; $Re = 80$; $Pr = 139.3$; $z = 75$; (1) $\theta = 0$, (2) $\theta = \pi$; (----) $z = 0$.

tion was used since the secondary flow velocity in the core is not zero. The results show that δ_θ is more important on the outer cylinder. It increases from $z = 0$ and tends asymptotically towards a constant value.

To show the axial development of the velocity and temperature fields, isotherms and isovalues of axial velocity were examined at different axial positions. Figure 7 shows isotherms and flow patterns for three axial locations: $z = 6.25$, 50 and 125, for $Gr = 6000$, $Pr = 557.3$, $Re = 35$ and $Pn = 0$. One can see that the isovalues of the axial velocity remain concentric circles along the heating zone. The axial flow is symmetric with respect to the horizontal axis. Indeed, Nieckele *et al.* [3] have shown by an appropriate scaling of the conservation equations that for large Prandtl number, the axial flow is not disturbed by natural convection. However, for fluid with lower Prandtl number, there is a reorganization of the flow, characterized by an increase of the axial velocity at the lower part of the annular duct and a decrease at the upper part (Figure 8). According to Yao [11], the axial velocity profile turns to accommodate the downward stream generated by the displacement of the secondary boundary layer. Next, the evolution of isotherms is examined (Figure 7). Near the entrance section, the isotherms are practically concentric circles (Figure 7(a)). The free convection is weak and the forced convection is the dominant mechanism. As the fluid moves from the entrance, the isotherms are gradually distorted (Figure 7(b) and (c)). They are closely spaced and nearly circular in the lower part of the cross-section, and sparsely spaced in the upper part. This indicates a deterioration of the heat transfer in the upper part of the annular duct and an improvement in the lower part. The evolution of the top and bottom wall temperatures of the outer cylinder is represented in Figure 9. It corresponds to the first region, described by Abid *et al.* [15], where the secondary flow develops. From $z \approx 125$, the thermal establishment starts with the developed dynamic regime. In this second region, the wall temperature increases linearly with z.

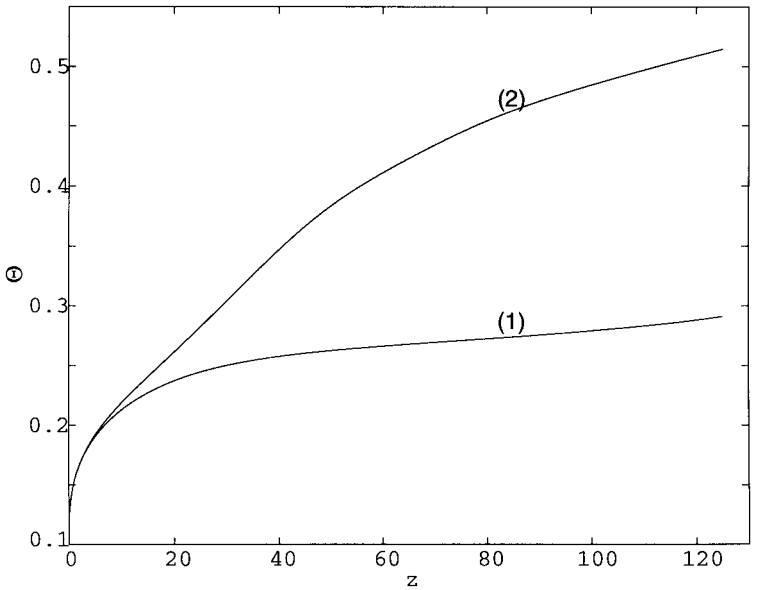

Figure 9. Evolution of the outer cylinder wall temperature along the heating zone. $Re = 35$; $Gr = 6000$; $Pr = 557.3$; $Pn = 0$; (1) $\theta = 0$, (2) $\theta = \pi$.

Having examined independently the effect of the variation of the viscosity with temperature and that of buoyancy on the structure of the flow, the problem of mixed convection with a thermodependence of the viscosity is now analyzed. As indicated previously, the decrease of μ with T, on one hand, reduces the drag forces of viscous origin, thereby increasing the intensity of the secondary flow, and on other hand increases the wall axial velocity gradient, which in

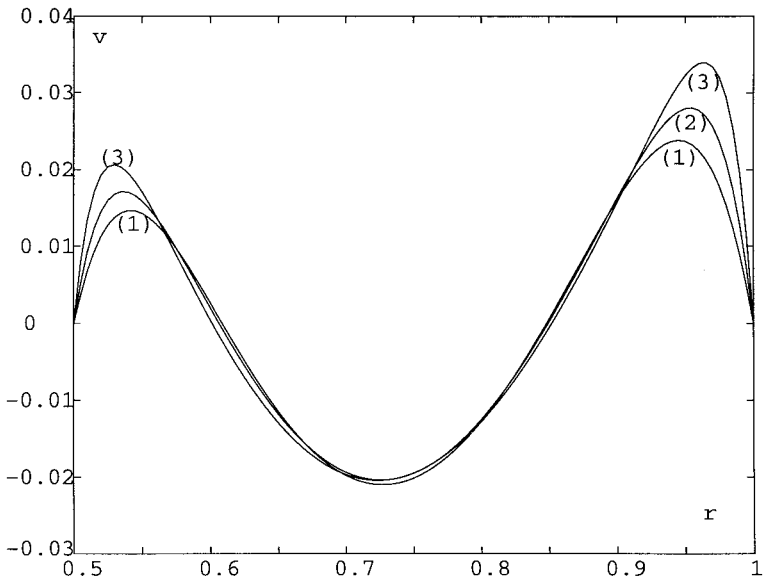

Figure 10. Effect of the Pearson number on the secondary flow: $\theta = \pi/2$; $z = 75$; $Re = 35$; $Gr = 6000$; $Pr = 557.3$; (1) $Pn = 0$, (2) $Pn = 4$, (3) $Pn = 10$.

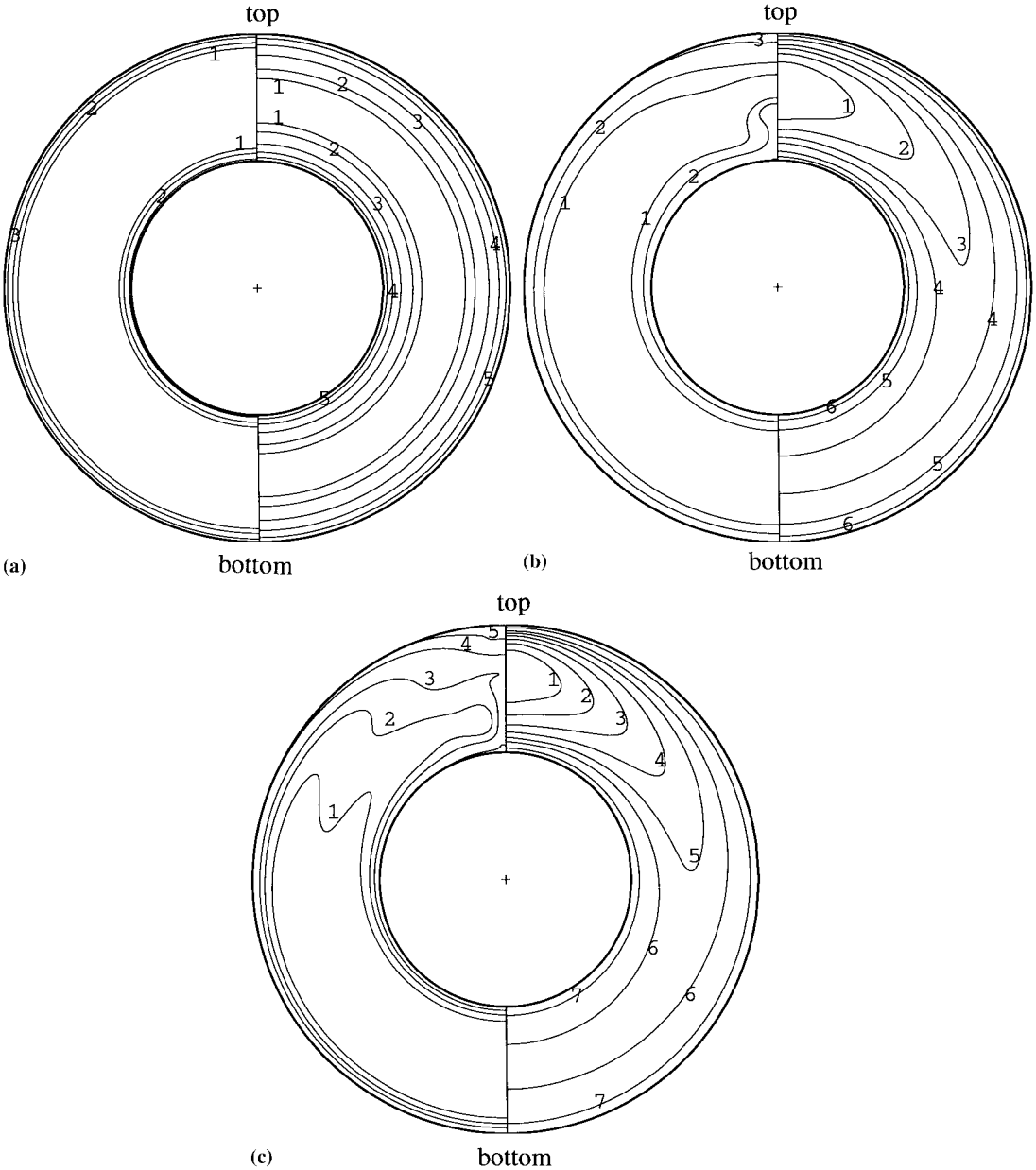

Figure 11. Isotherms (left-hand-side) and axial velocity contours (right-hand-side): $Re = 35$; $Gr = 6000$; $Pr = 557.3$; $Pn = 10$. (a) $z = 6.25$; isotherms: $\Theta_{max} - \Theta_e = 0.085$: (1) 0.1, (2) 0.3, (3) 0.7; iso-axial velocity (iso u/U_{max}): $U_{max} = 1.41$: (1) 0.9, (2) 0.8, (3) 0.6, (4) 0.4, (5) 0.2. (b) $z = 50$; isotherms: $\Theta_{max} - \Theta_e = 0.22$: (1) 0.1, (2) 0.3, (3) 0.7; iso-axial velocity: $U_{max} = 1.79$: (1) 0.9, (2) 0.8, (3) 0.6, (4) 0.4, (5) 0.2. (c) $z = 125$; isotherms: $\Theta_{max} - \Theta_e = 0.28$: (1) 0.1, (2) 0.2, (3) 0.3, (4) 0.5, (5) 0.7; iso-axial velocity: $U_{max} = 2.32$: (1) 0.9, (2) 0.8, (3) 0.6, (4) 0.4, (5) 0.2.

turn decreases the thermal boundary layer thickness, and therefore δ_θ. This result is illustrated in Figure 10, where tangential velocity profiles are represented at $\theta = \pi/2$, $z = 75$ and for three different values of $Pn = 0$, 4 and 10. The maximum of the tangential velocity v_{max}, increases with Pn and the radial position of v_{max} indicates that δ_θ decreases with Pn. The dynamic and

the thermal fields structures can be appreciated through Figure 11, where isotherms and axial velocity contours are represented for three axial locations $z = 6.25$, 50 and 125. Near the entry section ($z = 6.25$), the axial velocity contours are concentric circles; the forced convection is the dominant mechanism. Further downstream, the secondary flow due to the buoyancy term increases progressively and leads to the appearance of a low density fluid layer with a higher temperature at the upper part of the annular duct. The cold fluid is confined in the lower part. As μ decreases with T, the axial velocity increases at the upper part of the annular duct, as shown on Figure 11(b) and (c). Figure 12 shows clearly the acceleration of the fluid at $\theta = \pi$ and the deceleration at $\theta = 0$. At $z = 125$, $u(\theta = 0) = 1$ and $u(\theta = \pi) = 2.32$. Therefore, the classical assumption used by Hong and Bergles [7], which permits the consideration that the axial velocity is undisturbed by the secondary flow for large Prandtl numbers, is not valid when the fluid viscosity varies sufficiently with temperature. The distortion of the isotherms is similar to that for $\mu =$ constant. However, the temperature difference between the upper and lower part of annular duct decreases with Pn since the axial velocity is higher at $\theta = \pi$. Figure 13 shows for the outer cylinder, the evolution of $[\Theta(\theta = \pi) - \Theta(\theta = 0)]$ along the heated zone for different values of Pn. A similar but less pronounced result was obtained for the inner cylinder. According to Abid *et al.* [15], beyond a certain axial position z', which depends on Gr, Pe and Re, this temperature difference becomes constant, corresponding to the establishment of the thermal field.

Figure 14 shows the variation of the circumferentially averaged Nusselt number at the inner and the outer cylinders along the heated zone for $Pn = 0$ and 10. The broken lines correspond to forced convection. Two zones can be distinguished in the evolution Nu (X^+) for $Gr \neq 0$ (curves 3–5). In the first region (here $X^+ < X_c^+ \approx 10^{-3}$), the free convection effects are insignificant, and all the curves follow the forced convection curve. In the second region, $X^+ > X_c^+$, the buoyancy force becomes important, the curves for mixed convection rise above the forced convection curve. The comparison of the difference $[Nu(Gr = 6000, Pn = 0) - Nu(Gr = 0, Pn = 0)]$ curves 1 and 3, with $[Nu(Gr = 6000, Pn = 10) - Nu(Gr = 0, Pn = 10)]$

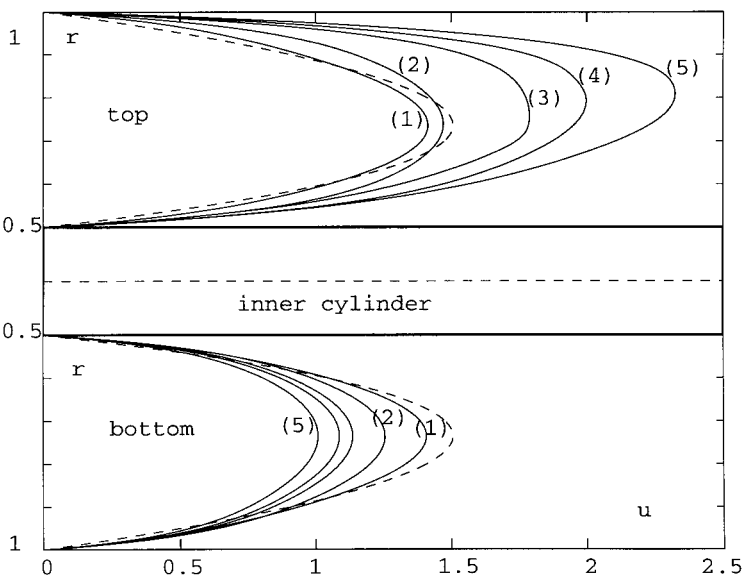

Figure 12. Evolution of the axial velocity profile along the heating zone: $Re = 35$; $Gr = 6000$; $Pr = 557.3$; $Pn = 10$; (----) $z = 0$; (1) $z = 6.25$, (2) $z = 25$, (3) $z = 37.5$, (4) $z = 50$, (6) $z = 75$.

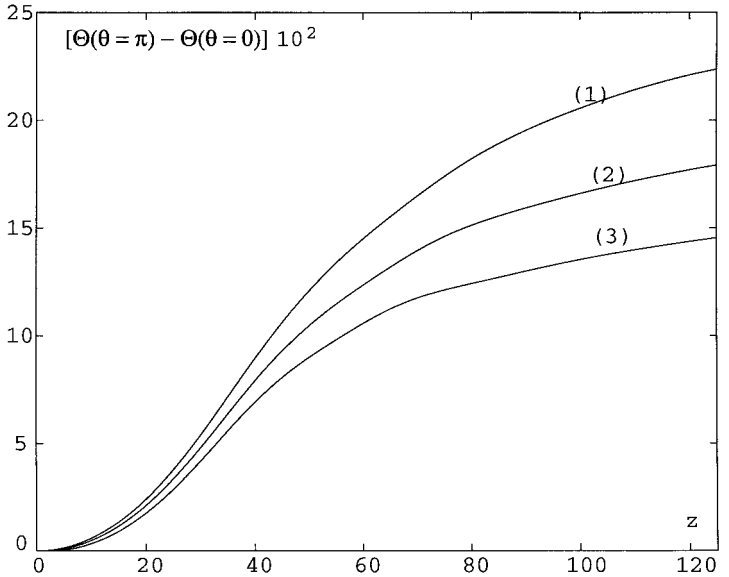

Figure 13. Dimensionless temperature difference between the top and the bottom of the outer cylinder along the heated region: $Re = 35$; $Gr = 6000$; $Pr = 557.3$; (1) $Pn = 0$, (2) $Pn = 4$, (3) $Pn = 10$.

curves 2 and 4, indicates that the increment of Nu with respect to the forced convection values increases with Pn because the secondary flow is more important. One can note also that the heat transfer is better on the inner than that on the outer one. Indeed, the numerical results show that the axial velocity gradient is higher on the inner wall. Concerning the X_c^+ location,

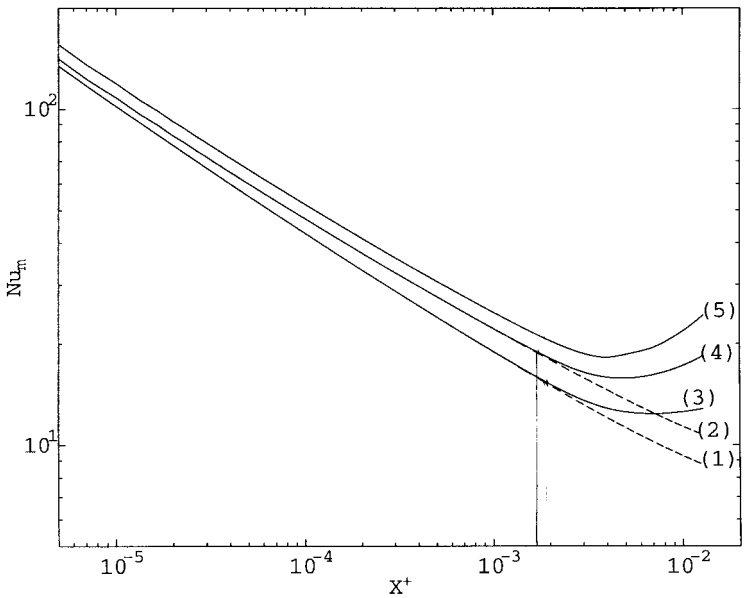

Figure 14. Circumferentially averaged Nusselt number: $Re = 35$; $Pr = 557.3$; (1) outer cylinder; $Gr = 0$, $Pn = 0$; (2) outer cylinder; $Gr = 0$; $Pn = 10$; (3) outer cylinder; $Gr = 6000$; $Pn = 0$; (4) outer cylinder; $Gr = 6000$; $Pn = 10$; (5) inner cylinder; $Gr = 6000$; $Pn = 10$.

where the Nu_m curve for mixed convection begins to depart from its forced convection counterpart, the calculations indicate, that X_c^+ shifts axially towards the entrance section when Gr increases. The effect of Pn on X_c^+ is similar to that of Gr, but it is less pronounced.

5. CONCLUSION

The effect of variable viscosity on laminar mixed convection in horizontal annular duct has been analyzed. The continuity equation and the three-dimensional parabolized form of the momentum and energy equations are solved numerically by the finite difference technique. Two regions have been distinguished, a first region near the entrance section where the forced convection is dominant, and a second region further downstream, where the secondary flow due to natural convection becomes stronger. The numerical results show that a decrease of μ with T induces: (i) intensification of the secondary flow and a reduction of the corresponding boundary layer thickness, (ii) an acceleration of the axial flow at the upper part of the duct and a deceleration at the lower part, by opposite to the case of constant viscosity; (iii) a reduction of the temperature difference between the top and bottom of a cylinder; (iv) an increase of the overall heat transfer in forced and mixed convection; (v) an axial displacement of X_c^+ towards the inlet.

REFERENCES

1. B.R. Morton, 'Laminar convection in uniformly heated horizontal pipes at low Rayleigh numbers', *Q. J. Mech. Appl. Mech.*, **12**, 410–420 (1959).
2. A. Mojtabi and J.P. Caltagirone, 'Analyse du transfert de chaleur en convection mixte laminaire entre deux cylindres coaxiaux horizontaux', *Int. J. Heat Mass Transf.*, **23**, 1369–1375 (1980).
3. A.O. Nieckele and S.V. Patankar, 'Laminar mixed convection in a concentric annuli with horizontal axis', *J. Heat Transf. ASME*, **107**, 902–909 (1985).
4. S. Kotake and N. Hattori, 'Combined forced and free convection heat transfer for fully developed laminar flow in horizontal annuli', *Int. J. Heat Mass Transf.*, **28**, 2113–2120 (1985).
5. M. Ciampi, S. Faggiani, W. Grassi, F.P. Incropera and G. Tuoni, 'Experimental study of mixed convection in horizontal annuli for low Reynolds numbers', *8th Int. Heat Transfer Conference*, San Francisco, CA, 1986, pp. 1413–1418.
6. O. Thermina, A. Mojtabi and B. Roux, 'A numerical procedure for three-dimensional mixed convection developing flows in an axisymetric geometry', *Eur. J. Mech. B/Fluids*, **11**, 21–38 (1992).
7. S.W. Hong and A.E. Bergles, 'Theoretical solutions for combined forced and free convection in horizontal tubes with temperature-dependent viscosity', *J. Heat Transf. ASME*, 459–465 (1976).
8. F.C. Chou and C.W. Tung, 'The mechanism of heat transfer enhancement for mineral oil in 2:1 rectangular ducts', *Int. J. Heat Mass Transf.*, **38**, 2863–2871 (1995).
9. S.D. Deshpande and D.B. Bishop, 'Heat transfer to non-Newtonian liquids flowing through tubes', *Chem. Eng. Comm.*, **52**, 339–354 (1987).
10. B. Shome and M.K. Jensen, 'Mixed convection laminar flow and heat transfer of liquids in isothermal horizontal circular ducts', *Int. J. Heat Mass Transf.*, **38**, 1945–1956 (1995).
11. L.S. Yao, 'Entry flow in a heated straight tube', *J. Fluid. Mech.*, **88**, 465–483 (1978).
12. S.V. Patankar and D.B. Spalding, 'A calculation for heat, mass and momentum transfer in three-dimensional parabolic flows', *Int. J. Heat Mass Transf.*, **15**, 1787–1806 (1972).
13. W.R. Briley, 'Numerical method for predicting three-dimensional steady viscous flows in ducts', *J. Comp. Phys.*, **14**, 8–28 (1974).
14. P.M. Worsoe-Schmidt, 'Heat transfer in the thermal entrance region of circular tubes and annular passages with fully developed laminar flow', *Int. J. Heat Mass Transf.*, **10**, 541–551 (1966).
15. C. Abid, F. Papini, A. Ropke and D. Veyret, 'Etude de la convection mixte dans un conduit cylindrique. Approches analytique/numérique et détermination expérimentale de la température de paroi par thermographie infrarouge', *Int. J. Heat Mass Transf.*, **37**, 91–101 (1994).

